

Cite this article as: Liu Tao, He Qing, Li Dan. Corrosion Resistance of Al₂O₃ Coating Prepared by Filtered Cathodic Vacuum Arc for Thermal Barrier Coatings Against CMAS Degradation[J]. Rare Metal Materials and Engineering, 2022, 51(11): 3981-3988.

ARTICLE

Corrosion Resistance of Al₂O₃ Coating Prepared by Filtered Cathodic Vacuum Arc for Thermal Barrier Coatings Against CMAS Degradation

Liu Tao^{1,2}, He Qing^{1,2}, Li Dan^{1,2}

¹ Surface Engineering Research Institute, Chinese Academy of Agricultural Mechanization Sciences, Beijing 100083, China; ² Beijing Golden Wheel Special Machine Co., Ltd, Beijing 100083, China

Abstract: To improve the deposit (the main components are CaO, MgO, Al₂O₃, and SiO₂, together referred to as CMAS) corrosion resistance of thermal barrier coatings (TBCs), the filtered cathodic vacuum arc (FCVA) technique was adopted to prepare a dense Al₂O₃ coating on the surface of TBCs. The wetting behavior and CMAS corrosion resistance of Al₂O₃-modified TBCs and as-deposited TBCs were compared and analyzed. Results show that the preparation of Al₂O₃ coating by FCVA technique has no obvious influence on the structure of 7wt% yttria-stabilized zirconia (7YSZ) phase. Besides, the Al₂O₃-modified TBCs have better comprehensive performance compared with the as-deposited TBCs. Under the CMAS corrosion at 1250 °C, the Al₂O₃ coating effectively restricts the spread of molten CMAS on TBC surface. In addition, the Al₂O₃ coating fills the gaps between 7YSZ columnar crystals and hinders the infiltration of molten CMAS. It is proved that FCVA method is appropriate to Al₂O₃ coating preparation in order to improve the CMAS corrosion resistance of TBCs, and the Al₂O₃ coating and its preparation do not have negative influence on the thermal shock performance of TBCs.

Key words: FCVA; Al₂O₃ coating; 7YSZ; CMAS

The thermal barrier coatings (TBCs) can protect the substrate from oxidation, improve the engine operating efficiency, and offer thermal insulation to the hot section components of advanced gas turbine. Commonly, TBCs consist of the MCrAlY bond coating, thermally grown oxide (TGO), and 7wt% yttria-stabilized zirconia (7YSZ) top coating^[1-3]. Owing to the high operating temperature (above 1200 °C), TBCs are vulnerable to the degradation by the molten composites (the main components are CaO, MgO, Al₂O₃, and SiO₂, together referred to as CMAS)^[4,5]. It is reported that the molten CMAS firstly penetrates the porous top coating and then solidifies after cooling. During the process, the thermal stress resulting from the thermal expansion mismatch between CMAS and TBCs is generated internally, thereby leading to the crack formation and final failure^[6-10]. In addition, the reaction of dissolution/re-precipitation between CMAS and TBCs can cause the

transformation of yttria-stabilized tetragonal (t')-zirconia into yttria-rich cubic of yttria-stabilized zirconia (c-YSZ) or yttria-depleted monoclinic of yttria-stabilized zirconia (m-YSZ). This phenomenon also induces the crack formation and yttria-stabilized zirconia (YSZ) spallation^[11].

To improve the CMAS corrosion resistance of TBCs, the dense Al₂O₃ coating on the surface of TBCs is a promising approach. The Al₂O₃ coating can act as an impermeable barrier or a sacrificial layer to prevent the penetration of molten CMAS^[12,13] into TBCs. Fan^[14] and Zhang^[15] et al prepared α -Al₂O₃ layer on the surface of TBCs by magnetron sputtering and vacuum heat treatment at 900 °C. It is found that the TBCs covered by α -Al₂O₃ have better CMAS corrosion resistance than the original TBCs do after isothermal tests at 1200 °C for 24 h. It is also observed that the α -Al₂O₃ layer partially fills the open pores and cracks in the 7YSZ top coating, therefore hindering the penetration of molten CMAS.

Received date: December 13, 2021

Foundation item: National Science and Technology Major Project (2017-VII-0007-0100)

Corresponding author: He Qing, Ph. D., Professor, Surface Engineering Research Institute, Chinese Academy of Agricultural Mechanization Sciences, Beijing 100083, P. R. China, E-mail: heqing@caams.org.cn

Copyright © 2022, Northwest Institute for Nonferrous Metal Research. Published by Science Press. All rights reserved.

Moreover, α -Al₂O₃ reacts with CMAS, forming the new compounds CaAl₂Si₂O₈ and MgAl₂O₄ with high melting points (above 1500 °C), which also play the role of resistance against CMAS infiltration. Mohan et al.^[16] prepared a dense and crack-free Al₂O₃ layer for TBCs by electrophoretic deposition technique and investigated the CMAS corrosion resistance of modified coatings at 1300 °C. It is found that the dense Al₂O₃ layer can react with CMAS to generate CaAl₂Si₂O₈ and MgAl₂O₄, which effectively improves the CMAS corrosion resistance of TBCs.

Currently, a large number of coating techniques, such as chemical vapor deposition (CVD), phase vapor deposition (PVD), plasma spray (PS), magnetron sputtering, and electrophoretic deposition technique, have been used to prepare the Al₂O₃ coatings for TBCs. Among these techniques, the filtered cathodic vacuum arc (FCVA) technique has been widely applied for the preparation of dense continuous crack-free coating due to the high ionization rate and free of macroparticle pollution^[17-19]. It is also reported that the FCVA process can be conducted at low temperature (~200 °C)^[20]. Hence, FCVA technique is suitable to deposit dense and impurity-free Al₂O₃ coating on the surface of TBC, avoiding the 7YSZ transformation during the depositing process.

In this research, the Al₂O₃ coating was prepared on the surface of TBC by FCVA technique. The wetting behavior and corrosion resistance against CMAS of Al₂O₃-modified TBCs and as-deposited TBCs were evaluated. The phase composition and microstructures of the coatings before and after corrosion were investigated. The performance difference of the coatings was analyzed. This research may offer a new approach to improve the CMAS corrosion resistance of TBCs.

1 Experiment

The TBC system used in this research consisted an electron-beam physical vapor deposited (EB-PVD) 7YSZ top coating, the GH 4169 superalloy sheets, and the NiCrAlY bond coating prepared by high-velocity oxygen fuel (HVOF) with commercial powders (99.9% purity, Institute of Metal Research, Chinese Academy of Sciences). The substrates sheets (25 mm×13 mm×1.5 mm) were previously grit-blasted with Al₂O₃ to improve the coating adhesion. The thickness of bond coating and top coating was about 20 and 150 μm, respectively. Al₂O₃ film was prepared on the TBC surface by FCVA technique with the thickness of 2 μm. The Al₂O₃ film was prepared by Al target (99.99% purity) and O₂ (99.999% purity) gas. Before deposition, the base pressure of the deposition chamber was evacuated to 3×10⁻³ Pa. The deposition chamber atmosphere and pressure were controlled by the O₂ gas inlet. The substrate temperature was controlled by the temperature controller system, and the thickness of the Al₂O₃ film was controlled by the deposition time. During the deposition process, the O₂ gas flow rate was 20 mL/min. The O₂ gas inlet was closed when the deposition chamber was evacuated to 2×10⁻² Pa. The direct current, working time, and deposition temperature was set 90 A, 1 h, and 200 °C, respectively. Finally, the Al₂O₃-modified 7YSZ coatings were

obtained.

CMAS was composed of 14.25mol% CaO, 4.81mol% MgO, 17.56mol% Al₂O₃, 48.88mol% SiO₂, and 3.02mol% TiO₂^[21]. The melting point of CMAS was measured by differential scanning calorimetry (DSC) as 1240 °C. CMAS (0.05 g) was compressed under the fixed pressure into the cylinder with height of 5 mm and diameter of 3 mm, and then placed on the Al₂O₃-modified TBC specimen. Subsequently, the overall specimen was fixed on an Al₂O₃ sample holder. Finally, the specimen was placed in the furnace center. The temperature was 1250 °C with a heating rate of 10 °C/min, and the specimen was kept at 1250 °C for 20 min. The morphology change of CMAS cylinder was supervised by the charge-coupled device (CCD) camera. Besides, the as-deposited TBCs were used as the control specimens for comparison.

The thermal shock performance of the Al₂O₃-modified TBCs and as-deposited TBCs was evaluated through the water quenching tests. The specimens were heated to 1100 °C and kept for 10 min in the furnace and then quenched by water to room temperature. The corrosion resistance against CMAS of Al₂O₃-modified and as-deposited TBCs was evaluated. The CMAS powders were uniformly brushed onto the surface of different specimens and the CMAS concentration was about 50 mg/cm². Then, the Al₂O₃-modified and as-deposited TBCs were placed in the air furnace and isothermally oxidized at 1250 °C for 2 h, which were denoted as A-TBCs and N-TBCs, respectively. The preheating/cooling rate of air furnace was set as 6 °C/min.

The phase composition of the specimens before and after tests were examined by X-ray diffraction (XRD, RAX-10, Rigaku, Japan) with Cu K α (λ =0.154 056 nm) radiation. The surface and cross-section morphologies of the specimens before and after tests were investigated by field emission scanning electron microscope (FE-SEM, S-4800, HITACHI, Japan). The chemical composition and element distributions of the specimens before and after tests were analyzed by the energy dispersive spectrometer (EDS, PN-5502, INCA ENGERY, UK)

2 Results and Discussion

2.1 XRD patterns of coatings

XRD patterns of the as-deposited and Al₂O₃-modified TBCs coatings are shown in Fig. 1. It can be seen that the as-deposited TBC prepared by EB-PVD is mainly composed of m-ZrO₂, c-ZrO₂, and t'-ZrO₂ phases. As for the Al₂O₃-modified TBC, no distinct peaks of Al₂O₃ can be observed, because the coating prepared by FCVA method is usually amorphous^[22-24].

2.2 Microstructure of coatings

Surface and cross-section morphologies of the as-deposited and Al₂O₃-modified TBCs are shown in Fig. 2. It can be seen from Fig. 2a that the surface morphology of the as-deposited TBC shows the typical columnar structure and the gaps between 7YSZ columnar crystals are obvious. EDS spectrum of point 1 in Fig. 2a demonstrates that the composition of the

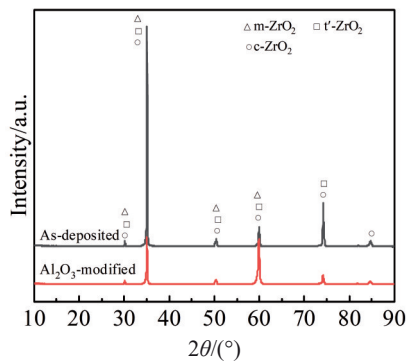


Fig.1 XRD patterns of as-deposited and Al_2O_3 -modified TBCs

top coating is mainly ZrO_2 , which is in accordance with the XRD results. The cross-section morphology of as-deposited TBC (Fig.2c) shows that the thickness of bond coating is $\sim 20\ \mu\text{m}$. Fig.2d shows that TGO appears with the thickness of $\sim 0.2\ \mu\text{m}$ due to the oxidation. Fig.2e and 2f prove that the ratio of Y:Zr is approximately 7:93. The roughness of as-deposited

TBC is 1.09. The surface morphology of Al_2O_3 -modified TBC (Fig. 2g) is denser than that of the as-deposited TBC, indicating that the Al_2O_3 coating is beneficial to protect the top coating from the penetration by molten CMAS^[25].

EDS spectrum of point 4 in Fig.2g shows that the element mainly contains the Al, Zr, and O. The structural characteristics of as-deposited TBC remain even after the deposition of Al_2O_3 coating. It can be seen that the structure of Al_2O_3 coating with the thickness of $\sim 2\ \mu\text{m}$ is integrated and consecutive and the Al_2O_3 coating completely fills the gaps between 7YSZ columnar crystals. The surface roughness of Al_2O_3 -modified TBC is 1.02, indicating that Al_2O_3 coating does not affect the roughness of TBCs.

The specimens after cooling process were observed by optical microscope (OM), and the geometries of CMAS pellets after heating and stabilization are illustrated in Fig.3. Obviously, the area occupied by the molten CMAS on as-deposited TBC (Fig. 3a) is larger than that on the Al_2O_3 -modified TBC (Fig.3b); the diameter of the as-deposited and Al_2O_3 -modified TBCs is 6.8 and 5.5 mm, respectively. Meanwhile, it can be seen that the contact angle of the as-

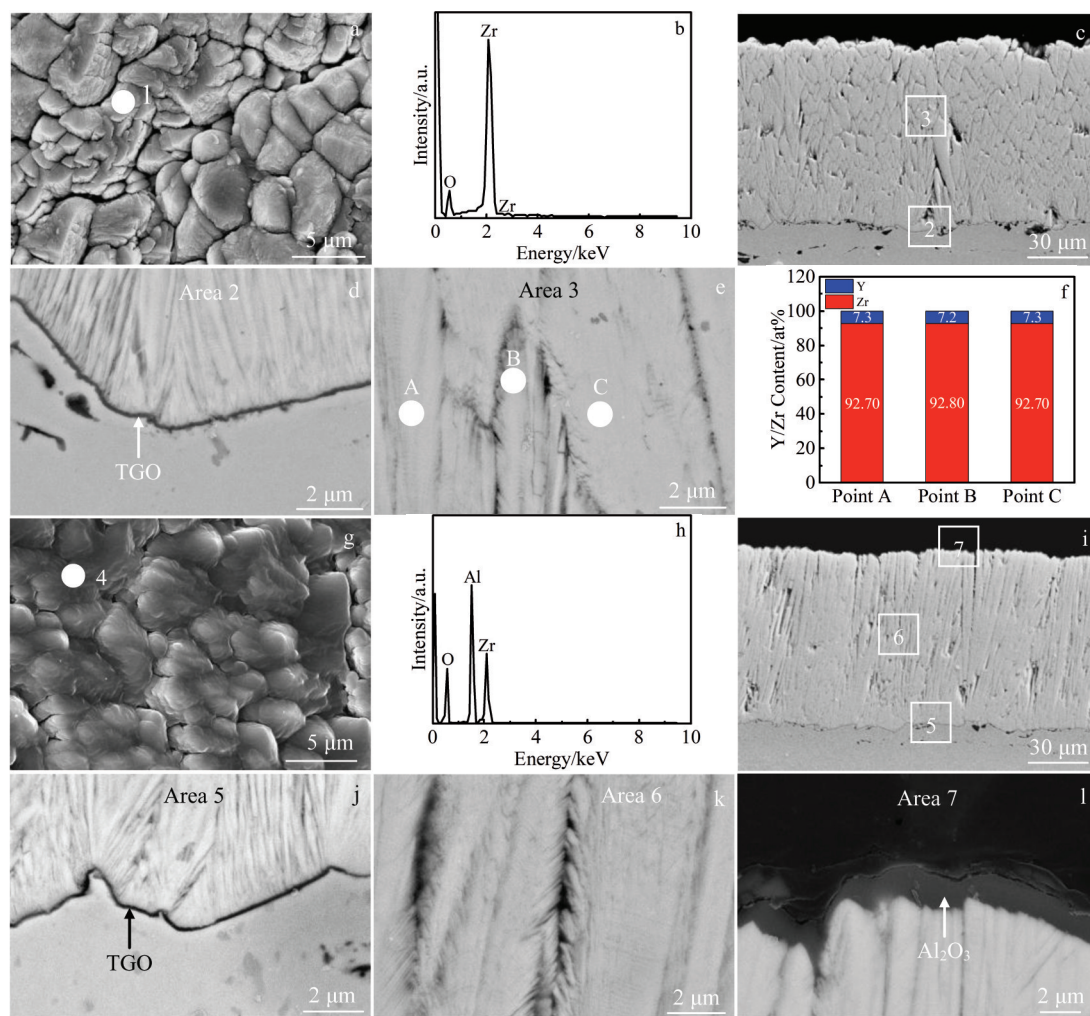


Fig.2 Surface (a, g) and cross-section (c, i) morphologies and EDS analysis results of as-deposited (a~f) and Al_2O_3 -modified (g~l) TBCs: (b) EDS spectrum of point 1 in Fig.2a; (d, e) magnified morphologies of area 2 and area 3 in Fig.2c, respectively; (f) EDS analysis result of point A~C in Fig.2e; (h) EDS spectrum of point 4 in Fig.2g; (j~l) magnified morphologies of area 5~area 7 in Fig.2i, respectively

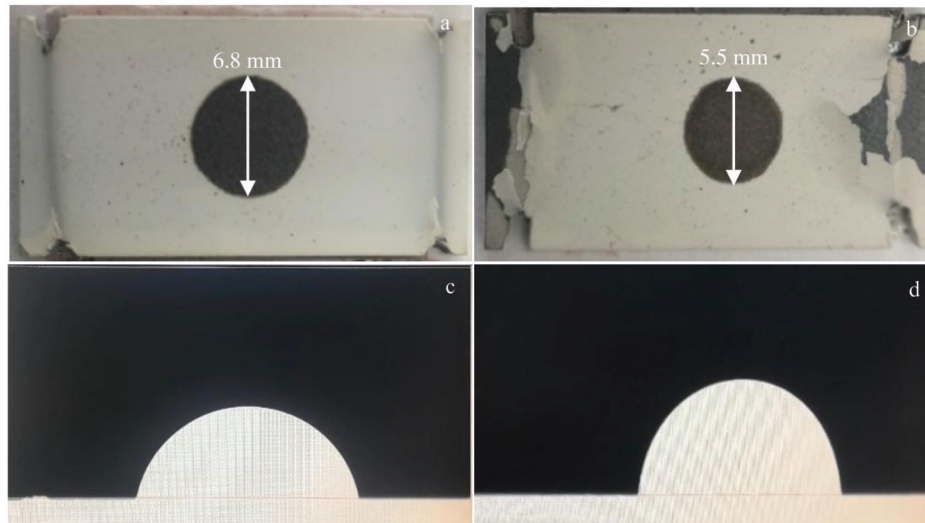


Fig.3 OM images (a, b) and contact angles (c, d) of as-deposited (a, c) and Al_2O_3 -modified (b, d) TBCs after wetting behavior tests

deposited TBC (Fig. 3c) is smaller than that of the Al_2O_3 -modified TBC (Fig. 3d). Therefore, it can be concluded that the molten CMAS is easier to spread on the surface of as-deposited TBCs, suggesting that the Al_2O_3 coating is beneficial to restrict the spread of molten CMAS.

The appearances of as-deposited and Al_2O_3 -modified TBCs after CMAS corrosion at $1250\text{ }^\circ\text{C}$ for 2 h are shown in Fig.4. As for N-TBC specimen, the as-deposited TBC fails^[11], indicating that the as-deposited TBCs cannot protect the substrate from corrosion for 2 h. The protective coating can still be found on the surface of A-TBC specimen after corrosion for 2 h, inferring that the corrosion resistance of Al_2O_3 -modified TBCs is better than that of as-deposited TBCs, i.e., the Al_2O_3 protective coating can significantly improve the corrosion resistance of TBCs. The grains of 7YSZ phase dissolve in the molten CMAS when the heating temperature is greater than $1190\text{ }^\circ\text{C}$ ^[26]. As for the N-TBC specimen, no barrier exists to resist the CMAS penetration during the dissolution/precipitation process. Thus, the molten CMAS penetrates the substrate through the open pores, cracks, and grain boundaries, i.e., TBCs fail during the CMAS corrosion. Because the Al_2O_3 film can fill the open pores and cracks of the top coating, the infiltration of molten CMAS is obviously hindered^[12]. When the heating temperature is greater than $1250\text{ }^\circ\text{C}$, CMAS is at the molten state and has good liquidity. Most CMAS is applied on the central area of TBC and a little molten CMAS is spread to the coating edge, thereby penetrating the interface between TGO layer and the ceramic coating. The grains of 7YSZ phase at TBC edge may dissolve into the molten CMAS and the TBC after corrosion is shed from the substrate. Besides, the stress change in the coating caused by the fast cooling rate also plays an important role in TBC shedding.

The surface and cross-section morphologies of as-deposited TBCs after CMAS corrosion at $1250\text{ }^\circ\text{C}$ for 2 h are shown in Fig.5. It can be seen that the coating surface is coarse and composed of different areas (Fig.5a). According to Fig.5b, the

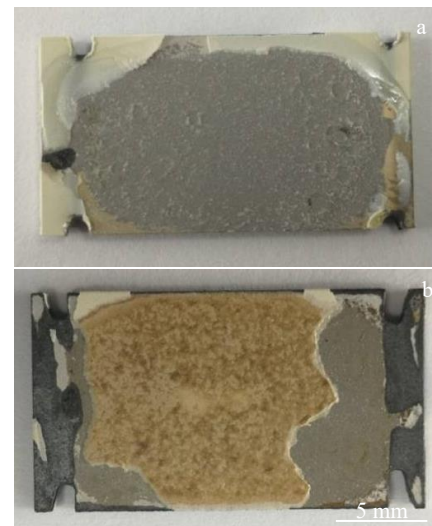


Fig.4 Appearances of as-deposited (a) and Al_2O_3 -modified (b) TBCs after CMAS corrosion at $1250\text{ }^\circ\text{C}$ for 2 h

light color area is composed of globular particles, which are identified as ZrO_2 by EDS spectrum in Fig.5c. In addition, the dark color area is composed of various elements (Fig. 5d), such as Ca, Si, Al, and Fe, indicating that the dark color area consists of solid CMAS after cooling process. Fig.5e shows the cross-section morphology of as-deposited TBC after CMAS corrosion. The penetrating crack can be clearly observed at the interface between TGO layer and bond coating. Furthermore, Fig.5f demonstrates that the substrate is no longer protected by the as-deposited TBC due to the spallation of coating, which is consistent with the appearance of N-TBC specimen.

Fig.6 displays the surface morphologies and EDS analysis results of Al_2O_3 -modified TBC after CMAS corrosion at $1250\text{ }^\circ\text{C}$ for 2 h. Evidently, the surface of Al_2O_3 -modified TBC (Fig.6a) consists of two phases. According to Fig.6b, it can be found that the area 1 is mainly composed of circular particles,

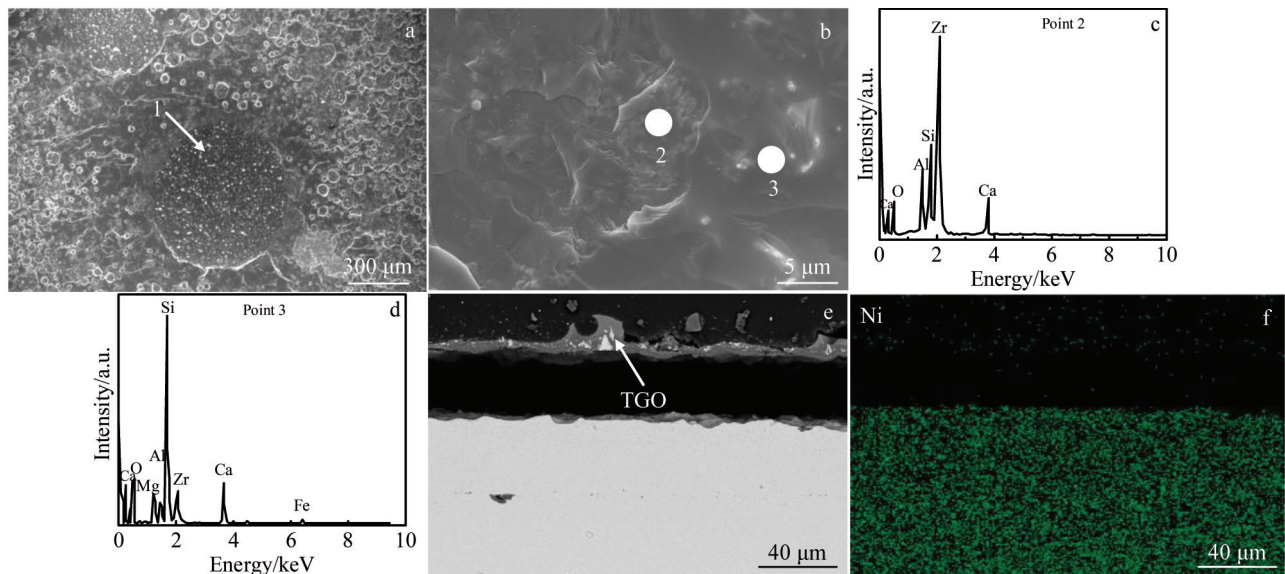


Fig.5 Surface (a) and cross-section (e) morphologies and EDS analysis results of as-deposited TBC after CMAS corrosion at 1250 °C for 2 h: (b) magnified morphology of area 1 in Fig.5a; (c, d) EDS spectra of point 2 and point 3 in Fig.5b, respectively; (f) EDS Ni element distribution corresponding to Fig.5e

which is identified as ZrO_2 by EDS spectrum in Fig. 6d. Meanwhile, the area 2 mainly consists of glassy substance, containing Ca, Mg, Al, Si, and Zr according to EDS spectrum in Fig.6e.

The cross-sectional morphologies and EDS line scanning results of Al_2O_3 -modified TBCs after CMAS corrosion at 1250 °C for 2 h are illustrated in Fig.7. It can be found that the 7YSZ phase structure of Al_2O_3 -modified TBC after CMAS corrosion (Fig. 7a) is basically consistent with that before CMAS corrosion (Fig.2i). However, the TGO layer (Fig.7a) is thickened in the Al_2O_3 -modified TBC after CMAS corrosion

owing to the oxidation, and its thickness is $\sim 15 \mu m$, which is obviously larger than that of TGO layer before CMAS corrosion ($0.2 \mu m$). Fig.7b shows EDS line scanning results of area 1 in Fig. 7a. It can be seen that O and Al elements are abundant in the area below 7YSZ top coating, promoting the thickening of TGO layer. Meanwhile, the elements, such as Ca, Mg, and Si, are dispersed homogeneously in the 7YSZ top coating. According to Fig.7c, it can be clearly observed that the thickness of protective Al_2O_3 coating is reduced, the integrity and continuity of the protective Al_2O_3 coating are broken, and the cracks appear after CMAS corrosion. Hence,

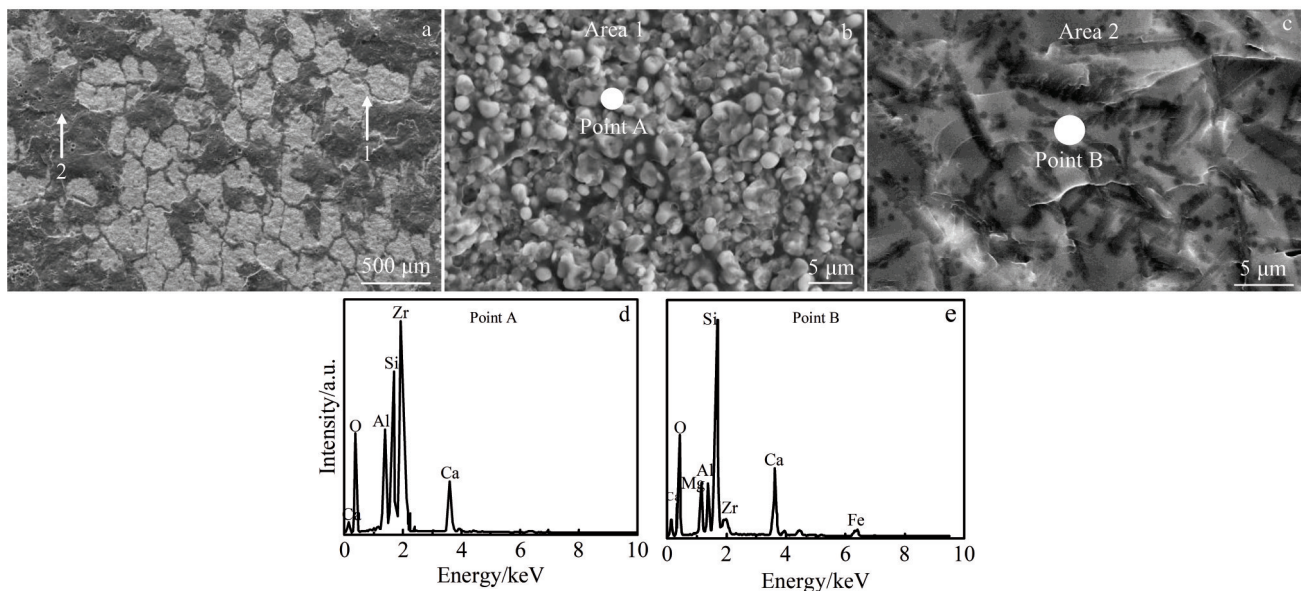


Fig.6 Surface morphology (a) and EDS spectra of Al_2O_3 -modified TBCs after CMAS corrosion at 1250 °C for 2 h: (b) magnified morphology of area 1 in Fig.6a; (c) magnified morphology of area 2 in Fig.6a; (d) EDS spectrum of point A in Fig.6b; (e) EDS spectrum of point B in Fig.6c

the structural change of Al_2O_3 coating after CMAS corrosion causes the gaps between 7YSZ columnar crystals to reopen. Then, some molten CMAS penetrates the substrate and is dispersed homogeneously in the 7YSZ top coating. However, it is worth noting that the atomic ratio of Y:Zr=8:92 in area 2 is basically the same as that in TBC before corrosion (7:93). Therefore, it can be concluded that the 7YSZ coating barely changes during CMAS corrosion process owing to the protection by Al_2O_3 coating. Fig. 7d shows that some cracks appear at the bottom of 7YSZ coating and the atomic ratio of Y:Zr=10:90 in this area is larger than that in area 1 (7:93), indicating that the c-YSZ phase appears after CMAS corrosion due to the reaction of dissolution/re-precipitation between CMAS and TBCs. The cracks appear at the interface between ceramic and bond coating in the Al_2O_3 -modified TBC^[27-29], as shown in Fig. 7d. On the one hand, when there is excess CMAS on the surface of TBC, yttria diffuses from TBC into the molten CMAS, resulting in the phase transformation in the 7YSZ phase. Besides, CMAS corrosion also results in the localized melting and subsequent re-precipitation of the coating, leading to the loss of columnar microstructures. The volume change during phase transformation and microstructure evolution leads to the stress change in the coating, thereby resulting in the generation of cracks. On the other hand, once the CMAS melts into TBCs and re-solidifies, the large thermal expansion mismatch between the CMAS layer and TBC occurs, the thermal stress is high, and the spallation of TBC occurs after cooling. The cracks appear at the interface between ceramic and bond coating, because a large amount of CMAS is infiltrated from the coating surface into interface. Fig. 7e and 7f show the Si and Ca element distributions in cross-section of Al_2O_3 -modified TBC after CMAS corrosion.

The water-quenching tests, namely the thermal shock

cycles, were conducted for as-deposited and Al_2O_3 -modified TBCs. Fig. 8 shows the surfaces of as-deposited and Al_2O_3 -modified TBCs during 60 cycles of quenching process from 1100 °C to room temperature. It can be seen that the as-deposited TBC begins to peel off after 30 thermal shock cycles. With increasing the thermal shock cycles, the shedding area becomes larger and larger, as shown in Fig. 8e. The color of Al_2O_3 -modified TBC surface becomes white (Fig. 8g) and the peeling phenomenon can be observed after 45 thermal shock cycles (Fig. 8i). The thermal shock performance of Al_2O_3 -modified TBCs is similar to that of the as-deposited TBCs because of the similar test life. Combined with the results obtained from XRD patterns, it is proved that the Al_2O_3 coating and its preparation process have no negative effect on performance of TBCs.

Based on the characterization results, it is believed that the as-deposited and Al_2O_3 -modified TBCs undergo different transformation processes during the CMAS corrosion. For the as-deposited TBCs, the porous columnar microstructure of 7YSZ top coating deposited by EB-PVD provides high strain tolerance, which is beneficial to extend the service life of TBCs^[30,31]. However, the gaps between 7YSZ columnar crystals provide channel for molten CMAS to enter into the TBCs during the CMAS corrosion process. Krmer et al^[9] found that the infiltrating molten CMAS is enriched at the interface between 7YSZ top coating and TGO layer, dissolves the underlying TGO layer, and promotes the generation of globular cubic ZrO_2 by dissolution/re-precipitation reaction between t'-YSZ phase and molten CMAS after heating at 1300 °C for 4 h. Hence, the TGO dissolution by CMAS and the thermal stress resulting from the phase transformation of t'-YSZ phase finally cause the separation of TBC from the substrate.

Compared with the as-deposited TBCs, the Al_2O_3 -modified

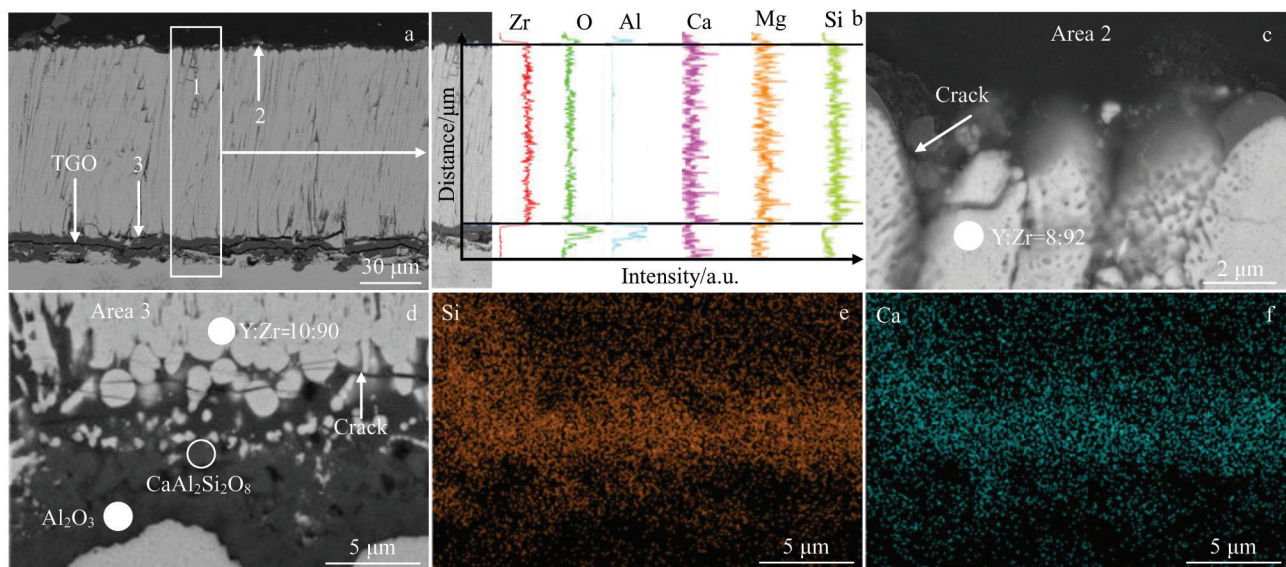


Fig.7 Cross-section morphology (a) and EDS analysis results of Al_2O_3 -modified TBCs after CMAS corrosion at 1250 °C for 2 h: (b) EDS line scanning results of area 1 in Fig.7a; (c, d) magnified morphologies of area 2 and area 3 in Fig.7a, respectively; (e, f) EDS Al element and Si element distribution corresponding to Fig.7d, respectively

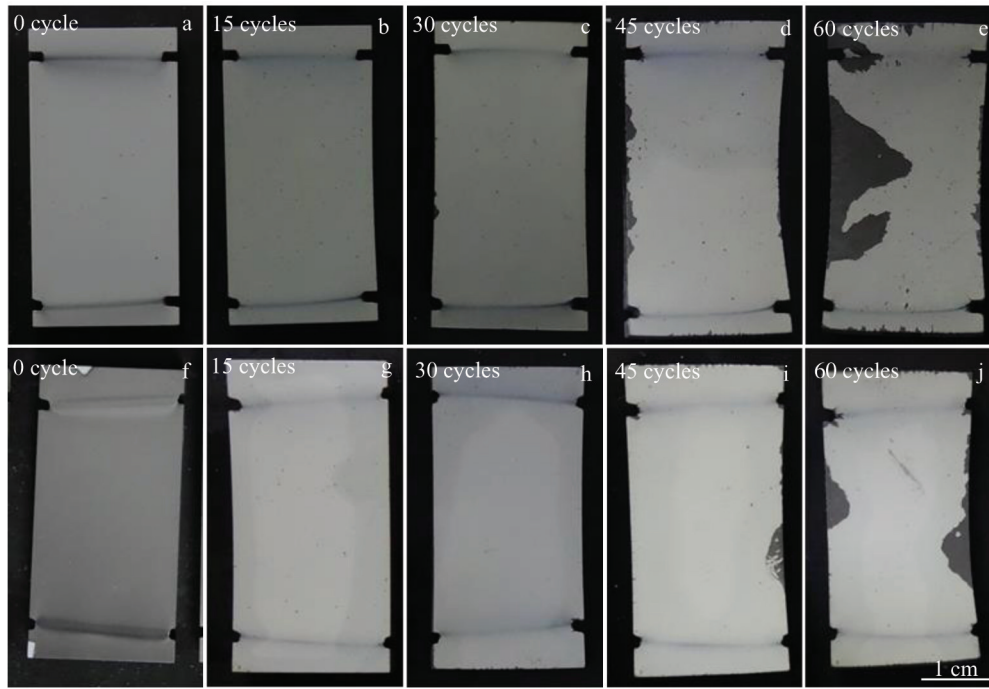


Fig.8 Thermal shock performance of as-deposited (a~e) and Al_2O_3 -modified (f~j) TBCs after thermal shock of 0 cycle (a, f), 15 cycles (b, g), 30 cycles (c, h), 45 cycles (d, i), and 60 cycles (e, j)

TBCs display superior CMAS corrosion resistance owing to the protective effect of Al_2O_3 coating prepared by FCVA technique. On the one hand, because the gaps between 7YSZ columnar crystals are filled by Al_2O_3 , the channels for CMAS penetration are decreased^[32-34]. On the other hand, the Al_2O_3 protective coating reacts with the molten CMAS, forming the protective anorthite with high melting point and resulting in good stability to hinder the further infiltration of molten CMAS into TBCs^[9,14-16]. However, with the consumption of Al_2O_3 , the thickness of Al_2O_3 coating is reduced and some gaps between 7YSZ columnar crystals reopen. Hence, a small amount of molten CMAS enters into the TBCs and is enriched at the interface between 7YSZ phase and TGO layer. Nevertheless, the destructive effect of molten CMAS is insufficient to cause the spallation between TBC and substrate after CMAS corrosion for 2 h.

3 Conclusions

1) The Al_2O_3 -modified thermal barrier coatings (TBCs) exhibit enhanced comprehensive performance, including larger contact angle, smaller spreading area, and better deposit (the main components are CaO, MgO, Al_2O_3 , and SiO_2 , together referred to as CMAS) corrosion resistance.

2) The preparation of Al_2O_3 coating has no negative influence on TBC performance. Al_2O_3 coating fills the gaps between the 7wt% yttria-stabilized zirconia (7YSZ) columnar crystals, therefore decreasing the channels for CMAS penetration. The Al_2O_3 coating can also react with the molten CMAS to form the protective anorthite.

3) The filtered cathodic vacuum arc (FCVA) technique is a suitable method to prepare Al_2O_3 coating in order to improve

the corrosion resistance of TBCs. The thermal shock performance of Al_2O_3 -modified TBCs is similar to that of the as-prepared TBCs because of the similar test life.

References

- 1 Miller R A. *Surface and Coatings Technology*[J], 1987; 30(1): 1
- 2 Bakan E, R Vaßen. *Journal of Thermal Spray Technology*[J], 2017, 26(6): 992
- 3 Chang F, Zhou K S, Tong X et al. *Applied Surface Science*[J], 2014, 317: 598
- 4 Borom M P, Johnson C A, Peluso L A. *Surface and Coatings Technology*[J], 1996, 86: 116
- 5 Vidal-Setif M H, Chellah N, Rio C et al. *Surface and Coatings Technology*[J], 2012, 208: 39
- 6 Mercer C, Faulhaber S, Evans A G et al. *Acta Materialia*[J], 2005, 53(4): 1029
- 7 Naraparaju R, Pubbysetty R P, Mechnich P et al. *Journal of the European Ceramic Society*[J], 2018, 38(9): 3333
- 8 Witz G, Shklover V, Steurer W et al. *Surface and Coatings Technology*[J], 2015, 265: 244
- 9 Krmer S, Yang J, Levi C G et al. *Journal of the American Ceramic Society*[J], 2010, 89(10): 3167
- 10 Yin B B, Zhang F, Zhu W et al. *Surface and Coatings Technology*[J], 2018, 357: 161
- 11 Pujol G, Ansart F, Bonino J P et al. *Surface and Coatings Technology*[J], 2013, 237: 71
- 12 Zhang X F, Zhou K S, Xu W et al. *Surface and Coatings Technology*[J], 2015, 261: 54

- 13 Guo Y Q, Wei L L, He Q et al. *Journal of Thermal Spray Technology*[J], 2021, 30(4): 864
- 14 Fan J F, Liu G, Zhuo X S et al. *Ceramics International*[J], 2021, 47(16): 22 404
- 15 Zhang X F, Zhou K S, Liu M et al. *Ceramics International*[J], 2016, 42(16): 19 349
- 16 Mohan P, Yao B, Patterson T et al. *Surface and Coatings Technology*[J], 2009, 204(6-7): 797
- 17 Zhou H, Shen Y Q, Huang J et al. *Applied Surface Science*[J], 2018, 440: 448
- 18 Liao B, Ouyang X P, Zhang X et al. *Journal of Materials Engineering and Performance*[J], 2018, 27(1): 72
- 19 Guan J J, Wang H Q, Qin L Z et al. *Nuclear Instruments and Methods in Physics Research: Section B*[J], 2017, 397: 86
- 20 Zhao Z W, Tay B K, Yu G Q et al. *Thin Solid Films*[J], 2004, 447: 14
- 21 Naraparaju R, Schulz U, Mechnich P et al. *Surface and Coatings Technology*[J], 2014, 260: 73
- 22 Olarinoye O, Ogundare F. *International Journal of Materials Research*[J], 2015, 106(5): 514
- 23 Shiiyama K, Howlader M R, Zinkle S J et al. *Journal of Nuclear Materials*[J], 1998, 258: 1848
- 24 Konstantinidis S, Jiang K, Roobroek A et al. *Plasma Processes and Polymers*[J], 2011, 8(7): 651
- 25 Song J B, Zhang X F, Deng C M et al. *Ceramics International* [J], 2016, 42(2B): 3163
- 26 Wu J, Guo H B, Gao Y Z et al. *Journal of the European Ceramic Society*[J], 2011, 31(10): 1881
- 27 Wellman R, Whitman G, Nicholls J R. *International Journal of Refractory Metals and Hard Materials*[J], 2010, 28(1): 124
- 28 Chen X. *Surface and Coatings Technology*[J], 2006, 200(11): 3418
- 29 Guo D, Yu Q M, Cen L. *Rare Metal Materials and Engineering* [J], 2020, 49(9): 2937
- 30 Keller I, Naumenko D, Quadackers W J et al. *Surface and Coatings Technology*[J], 2013, 215: 24
- 31 Song P, Naumenko D, Vassen R et al. *Surface and Coatings Technology*[J], 2013; 221: 207
- 32 Zhang X F, Zhou K S, Wei X et al. *Ceramics International*[J], 2014, 40(8): 12 703
- 33 Zhang X F, Zhou K S, Xu W et al. *Surface and Coatings Technology*[J], 2015, 261: 54
- 34 Zhang X F, Zhou K S, Dong S J et al. *Transactions of Nonferrous Metals Society of China*[J], 2015, 25(8): 2587

基于磁过滤技术的热障涂层表面 Al_2O_3 覆盖层抗 CMAS 腐蚀性能

刘涛^{1,2}, 何箐^{1,2}, 李丹^{1,2}

(1. 中国农业机械化科学研究院 表面工程技术研究所, 北京 100083)

(2. 北京金轮坤天特种机械有限公司, 北京 100080)

摘要: 为了提高热障涂层 (TBC) 的抗沉积物 (主要成分为 CaO 、 MgO 、 Al_2O_3 和 SiO_2 , 简称 CMAS) 腐蚀性能, 采用磁过滤阴极真空电弧 (FCVA) 技术在 TBC 表面上制备了致密的 Al_2O_3 覆盖层, 比较和分析了 Al_2O_3 改性 TBC 和沉积态 TBC 的润湿行为和抗 CMAS 腐蚀性能。结果表明: 使用 FCVA 技术制备 Al_2O_3 覆盖层的过程对 7% (质量分数) 氧化钇稳定的氧化锆 (7YSZ) 相的结构无明显影响, 且经 Al_2O_3 改性的 TBC 综合性能均优于沉积态 TBC。在 1250 °C、CMAS 腐蚀条件下, Al_2O_3 覆盖层有效地限制了熔融 CMAS 在 TBC 表面上的扩散行为。同时, Al_2O_3 填充了 7YSZ 柱状晶之间的间隔并且阻碍了熔融 CMAS 的渗透, 证明了 FCVA 可作为一种制备 Al_2O_3 涂层的新方法以提高 TBC 的抗 CMAS 腐蚀性能, 且 Al_2O_3 涂层及其制备过程对 TBC 的热震性能均无消极影响。

关键词: 磁过滤真空电弧; Al_2O_3 覆盖层; 氧化钇稳定的氧化锆; CMAS

作者简介: 刘涛, 男, 1988 年生, 博士, 工程师, 中国农业机械化科学研究院表面工程技术研究所, 北京 100083, 电话: 010-64882594, E-mail: 10607618aaa@163.com